Application of cellular automata to *N*-body systems

A. Lejeune
Institut de Physique B.5, Université de Liège, Sart Tilman, B-4000 LIEGE 1, Belgium

J. Perdang
Institute of Astronomy, Madingley Road, Cambridge CB3 OHA, United Kingdom
and Institut d'Astrophysique E.1, Université de Liège, 5, Avenue de Cointe, B-4000 Liege, Belgium

J. Richert
Laboratoire de Physique Théorique, Université Louis Pasteur, 3, Rue de l'Université, F-67084 Strasbourg Cedex, France
(Received 2 April 1999)

A two-dimensional cellular automaton model is introduced to deal with the dynamics of a finite system of particles whose interactions are simulated by two-body step potentials. The method is illustrated for a potential approximating the standard Lennard-Jones potential, representative for the problem of heavy ion collisions in nuclear physics. From the cellular automaton dynamics thermodynamic equibrium state variables are introduced in the usual way. The numerical experiments indicate the occurrence of a phase transition. Macroscopically the transition is marked by a singularity in the equation of state; microscopically it manifests itself by the formation of clusters of particles of all sizes, obeying a mass distribution in the form of a power law of exponent 1.35. [S1063-651X(99)04909-0]

PACS number(s): 05.40.−a, 05.45.−a, 25.70.−z

I. INTRODUCTION

We develop in this paper a multipurpose, multiparameter two-dimensional (2D) cellular automaton (CA) scheme devised to deal with *N*-particle systems. The particles interact dynamically through radial pair potentials, in accordance with classical mechanics. In the present version the particles themselves are conserved in the interaction; we anticipate, however, that reaction processes could be added without complicating the formulation in any basic way. The CA approach may be viewed as a discretized version of classical molecular dynamics (CMD), with the difference that several quantum-mechanical effects are introduced (exclusion principle, quantum-mechanical scattering). Like the latter, the CA approach lends itself to direct dynamical calculations from which statistical properties may be derived. In particular, thermodynamic properties may be obtained, provided that the conditions of thermal equilibrium are observed to be satisfied. The main advantage of the CA scheme with respect to CMD lies in its algorithmic simplicity. This implies in turn that the CA calculations are less time consuming, and, therefore, they lend themselves to investigations of broad parameter ranges, which can be explored with a small enough step. This point is of relevance in particular when phase transitions and other parameter-dependent phenomena are to be investigated. The price to be paid for the increase of computational efficiency is a decrease in the precision of the the individual particle trajectories. By the very construction of the CA framework the latter are not meaningful individually, but the statistical features of the ensemble of particles are properly represented. To some extent, a similar observation also holds for CMD; on the one hand, the trajectories of the particles in the treatment of CMD are not meaningful either, since the particles should be treated as quantum-mechanical objects in the first place; on the other hand, even in the strict classical context, the particle motions are chaotic, of very short Lyapunov time (of the order of the mean collision time); accordingly, we are unable in principle to compute the individual particle trajectories correctly over macroscopically relevant time scales.

The first part of this paper supplies a general discussion of our CA method. Besides the specific CA schematization (discrete time, cellular space, number of velocity states equal to the number of neighborhood cells, and Fermion-type exclusion principle), the following additional ingredients enter our model: (i) The calculations are two-dimensional; the particles are confined to a fixed ''volume'' (an area of the cellular lattice). (ii) Two-body interactions are taken into account, in the form of a multistep potential. (iii) Scattering probabilities are obtained quantum mechanically, from the potential discussed under (ii) above. (iv) Thermodynamic properties are derived following the methods of [2].

In the Sec. V we illustrate the approach by a specific nuclear *N*-body problem [1], which serves the main purpose of demonstrating the efficiency of the approach. We analyze the question of heavy ion collisions and the subsequent nuclear fragmentation. The method enables us to recover qualitatively known results (power law of the nuclear fragments); it also suggests a phase transition towards the formation of ''clusters'' of nucleons of different sizes. Since the calculations are two-dimensional, the results are not directly quantitatively comparable with actual experiments.

II. CA FRAMEWORK OF THE MODEL— THE LATTICE PAIR INTERACTION

In our model, time is measured by an integer multiple t of a basic time step $\Delta\tau$. The cellular space adopted is a regular hexagonal lattice space; the length of a side of a cell is re-

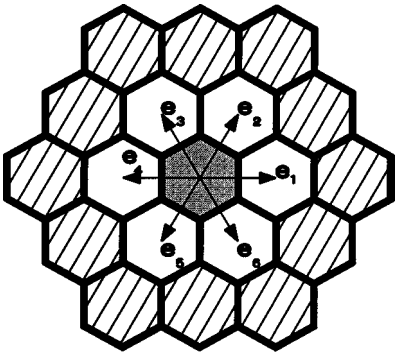

FIG. 1. Effective range of interactions included in CA dynamics: a nucleon in a reference cell (grey) interacts with any nucleon of the reference cell, the first ring (white cells), and the second ring of cells (hatched) surrounding the reference cell; unit vectors $\mathbf{e}_i$, $i=1,2,\ldots,6$, directions of velocities of moving states.

ferred to as the cellsize Δx; a cell is identified by the position vector $\mathbf{r}$ of its center.

A lattice particle, at time t and in cell $\mathbf{r}$, may be viewed as being smeared out over the cell, or, alternatively as a point occupying the cell center. It exists in one among seven momentum states: a particle is either at rest (state 0) or it is in a state of motion with a reference speed $|\mathbf{v}|$ in a direction $\mathbf{e}_i$ from the center of the cell $\mathbf{r}$ it occupies to the center of one of the six contiguous cells (position vectors $\mathbf{r}+l\mathbf{e}_i$); the directions $\mathbf{e}_i$ are labeled counterclockwise by the integer $i=1,2,\ldots,6$; $l=\sqrt{3}\Delta x$ is the distance between the centers of any pair of contiguous cells (Fig. 1).

The reference speed $|\mathbf{v}|$ is such that in one time step a moving particle is shifted to a contiguous cell,

$$|\mathbf{v}|=\frac{l}{\Delta\tau}. \tag{1}$$

Following a convention standard in lattice-gas dynamics since the work by Hardy *et al.* [3], a formal (computational) exclusion principle is adopted in the form that a spatial site carries at most one particle of each dynamical state; the number density allowed in our model then obeys the inequality $n(\mathbf{r})\leqslant 7$ particles per cell. This principle mimics to some extent the actual Pauli exclusion principle, thereby introducing a quantum-mechanical element into an otherwise classical model.

The model contains a total number A of identical particles, of mass m. These particles are conserved in the dynamics. We denote them by $A_r(t)$ and $A_m(t)$, the total number of rest and moving particles, respectively, at time t; hence, $A=A_r(t)+A_m(t)$.

Finally, we require the particles to be confined to a finite region of the lattice, of two-dimensional ''volume'' v. The boundary conditions for the particle motions are periodicity conditions.

In the illustration $\Delta\tau$ is chosen of the order of the collision time of nucleons in the bound nucleus ($\approx 10^{-23}$ s). Δx is of the order of the range of the nuclear forces (≈ 2 fm).

The general model pair potential we consider here is defined as follows. Let particle j occupy a central cell of position $\mathbf{r}_j$; denote by $R_1(\mathbf{r}_j)$ a first ring of cells surrounding the central cell; this ring is made up of the cells of positions defined by $\mathbf{r}_j+l\mathbf{e}_i$, $i=1,2,\ldots,6$; denote by $R_2(\mathbf{r}_j)$ a second ring of next-nearest neighbor cells, $\mathbf{r}_j+2l\mathbf{e}_i$ and $\mathbf{r}_j+l\mathbf{e}_i+l\mathbf{e}_{i-1}$, $i=1,2,\ldots,6$ (0 identified with 6), surrounding the first ring, etc. (Fig. 1).

The interaction potential between a pair of particles j,k, j, and k being in *different* cells, is represented by

$$V_{\text{pair}}(|\mathbf{r}_j-\mathbf{r}_k|;p)=V_s \quad \text{if}$$
$$\mathbf{r}_k\in R_s(\mathbf{r}_j); \quad s=1,2,3,\ldots,S,S+1,\ldots; \tag{2}$$

$V_1, V_2, \ldots, V_S, V_{S+1}, \ldots$ are adjustable parameters. In practice the interactions are of finite range, so that we then have $V_s=0$ if $s>S$. The argument p denotes the number of different pairs contained in the central cell $\mathbf{r}_j$ (allowed values: $p=1$, 3, 6, 10, 15, and 21), if the cell contains more than one particle; such a situation will be referred to as a ''collision state.'' While irrelevant if particles j and k are in different cells, this parameter becomes important when both particles are in the same cell; it enables us to simulate short-distance interactions with an improved precision. In case cell r_j is in a collision state, with both particles j and k in the *same* cell r_j, we set

$$V_{\text{pair}}(|\mathbf{r}_j-\mathbf{r}_k|;p)=V_{o,p} \quad \text{if} \quad \mathbf{r}_k=\mathbf{r}_j, \tag{2a}$$

where $V_{o,p}$, $p=1$, 3, 6, 10, 15, and 21 is again a collection of six extra adjustable parameters.

The total potential acting on a particle j at site $\mathbf{r}_j$ will be denoted by $V(\mathbf{r}_j;p)$. We have

$$V(\mathbf{r}_j;p)=\sum_{k\neq j} V_{\text{pair}}(|\mathbf{r}_j-\mathbf{r}_k|;p). \tag{3}$$

The potential acting on a particle j at site $\mathbf{r}_j$ and due to the particles in the neighboring cells only (rings $R_1, R_2, \ldots$, will be denoted by $V(\mathbf{r}_j)$:

$$V(\mathbf{r}_j)=\sum_{k\in R_1,R_2,\ldots} V_{\text{pair}}(|\mathbf{r}_j-\mathbf{r}_k|;p). \tag{3a}$$

The total potential (potential energy per particle mass) W is

$$W=\sum_{\text{pairs (j,k)}} V_{\text{pair}}(|\mathbf{r}_j-\mathbf{r}_k|;p), \tag{4}$$

the summation extending over all distinct pairs.

The total kinetic energy (per particle mass) is

$$K=\tfrac{1}{2}|\mathbf{v}|^2A_m. \tag{5}$$

In our nuclear-collision illustration the following numerical values for the parameters of the potential are adopted:

$$V_1=-10 \text{ MeV}, \quad V_2=-1 \text{ MeV} \quad \text{with}$$
$$V_s=0 \quad \text{for} \quad s\geqslant 3;$$
$$V_{o,p}=-10+(p-1)6 \text{ MeV}; \quad p=1,3,6,10,15,21. \tag{6}$$

With this choice of parameters the potential of a single pair in a cell corresponds to an attraction, while for two pairs

in a same cell the potential is already repulsive. The distance between adjacent cells is taken as $l=2.1$ fm.

We observe that the potential we adopt for our illustration generalizes the simplest lattice potential so far considered in the context of nuclear fragmentation (on a three-dimensional cubic lattice) by a variety of authors [1,4–7], namely, the one-parameter potential

$$V_{\text{pair}}(|\mathbf{r}_j-\mathbf{r}_k|)=-\epsilon \quad \text{if} \quad \mathbf{r}_k=\mathbf{r}_j+l\mathbf{e}_i,$$
$$i=1,2,\ldots$$
$$V_{\text{pair}}(|\mathbf{r}_j-\mathbf{r}_k|)=0 \quad \text{otherwise.} \tag{7}$$

This representation refers to a cubic lattice whose sites are allowed to carry either zero or one particle; the interaction potential is nonzero and attractive ($\epsilon>0$) only if the two particles are in adjacent cells.

CA EVOLUTION RULES

Given the CA configuration (i.e. the states of the collection of all cells) at time step t, a new configuration, at step $t+1$ is obtained by updating first all linear momenta, and then all positions.

The updating of the momenta is made (a) by taking account of the local collisions and then (b) by dealing with the finite range forces.

A. Collision phase

1. Local collisions

A local collision state C transforms into another allowed local collision state C' ($\neq C$), $C\rightarrow C'$, with probability $P_{CC'}\geqslant 0$ per time step, provided that the collision process satisfies energy-momentum conservation; the transition $C\rightarrow C'$ is forbidden, $P_{CC'}\equiv 0$, if energy–momentum conservation is violated. The nonzero transition probabilities $P_{CC'}$ are functions of the parameters $V_{o,p}$ of the interaction potential. These probabilities are computed by a preliminary standard scattering analysis of particles interacting through potential (3a) [8].

In our specific nuclear collision illustration the probabilities are obtained as follows. If C is a local collision state of a hexagonal cell, then a different collision state C' (out channel) exists only if state C contains one pair of opposite momenta, say in the direction $\mathbf{e}_i$ (momenta $\mathbf{e}_i$, $\mathbf{e}_{i+3}=-\mathbf{e}_i$, $i=1$, 2, or 3); denote this binary collision (sub)state by c; there are then at most two equivalent exit channels, namely, those with opposite momenta in the two directions $\mathbf{e}_j$, $j=i+1$, and $i-1$; we denote these binary states by c' and c''. The transition probabilities $P_{cc'}$, $P_{cc''}$, and P_{cc}, of the processes $c\rightarrow c'$, $c\rightarrow c''$, and $c\rightarrow c$, are related by

$$P_{cc''}\equiv P_{cc'} \quad \text{and} \quad P_{cc}=1-2P_{cc'}. \tag{8}$$

Only one among these three parameters is independent. If state C is a binary state ($=c$), then the quantum-mechanical diffusion probability for the typical numerical parameters we have adopted yields $P_{cc'}=0.42$.

If C is a higher-order collision state, we reduce the treatment in a straightforward way to considerations of binary substates c; for C ternary, the diffusion probability for our numerical parameters is reduced by a factor of the order of 100, as compared to our binary case; we, therefore, disregard this diffusion. For the higher-order collision states C, as a consequence of the exclusion principle, most out channels are closed. Although the diffusion probabilities (for the numerical parameters chosen) increase now with the number of particles per cell, the contribution of these diffusion probabilities to the dynamics is found to be inefficient. Therefore, in the actual computations these probabilities are disregarded.

2. Finite-range collisions

The momentum change $\Delta\mathbf{p}$ of a particle in cell $\mathbf{r}$ at time step t, due to the interactions with the rest of the particles in the neighboring cells [those in the same cell being treated under Eq. (3.1a)], is given by a discretized version of Newton's equation of motion

$$\Delta\mathbf{p}=\mathbf{F}(\mathbf{r})\Delta\tau; \tag{9}$$

$\mathbf{F}(\mathbf{r})$ represents the force acting on the particle in cell $\mathbf{r}$, which is due to the configuration of all other particles at time step t within the rings R_1, R_2, . . . ,R_S. We define the Cartesian force component at time step t in the lattice direction $\mathbf{e}_j$, $F_j(\mathbf{r})$, in terms of the forward difference of the potential at time t in the direction $\mathbf{e}_j$, i.e.,

$$F_j(\mathbf{r})=-\frac{m}{l}[V(\mathbf{r}+l\mathbf{e}_j)-V(\mathbf{r})], \tag{10}$$

where the potential at site $\mathbf{r}$ is given by Eq. (3a).

The remainder of the CA-adapted treatment of the force is a simplified version of the algorithm described in [9]. At time step t the particle has a momentum $\mathbf{p}$ which is either 0, or equal to $p\mathbf{e}_i$, $i=1,2,\ldots$, or 6, with $p=m|\mathbf{v}|$. The change of momentum $|\Delta\mathbf{p}|$, over one time step $\Delta\tau$, as given by the equation of motion [Eq. (9)], should be small as compared to $|\mathbf{p}|$; this computational requirement constrains the choice of the time step for a given lattice size. The formal momentum at time step $t+1$ becomes

$$\mathbf{p}'=\mathbf{p}+\Delta\mathbf{p}\equiv\mathbf{p}'_i+\mathbf{p}'_j. \tag{11}$$

If the momentum at time step t is nonzero, ($\mathbf{p}=p\mathbf{e}_i$), then the new momentum $\mathbf{p}'$ lies in the angular sector ($\mathbf{e}_i$,$\mathbf{e}_j$), $i=1,2,\ldots$, or 6, $j=i\pm 1$. Represent then $\mathbf{p}'$ as the sum of the two vectors $p'_i\mathbf{e}_i$, $p'_j\mathbf{e}_j$ directed along the axes $\mathbf{e}_i$, $\mathbf{e}_j$ (Fig. 2); the absolute value of $\mathbf{p}'$ remains close to p, so that $p'_i\approx p$ and $p'_j\ll p$.

If the momentum at step t is zero, then the directions $\mathbf{e}_i$ and $\mathbf{e}_j$ are chosen to flank the force direction. The right-hand side of Eq. (11) now represents the vectorial decomposition of $\Delta\mathbf{p}$ along the skew axes $\mathbf{e}_i$, $\mathbf{e}_j$; hence, we have $p'_i\ll p$ and $p'_j\ll p$.

Since our CA model has only seven momentum states, we have to reset the new momentum $\mathbf{p}'$ equal to one of these admissible states:

$$\mathbf{p}'\rightarrow\mathbf{p}''=0, \quad (P_o) \quad \text{or} \quad p\mathbf{e}_k, \quad (P_k), \quad k=1,2,\ldots,6. \tag{12}$$

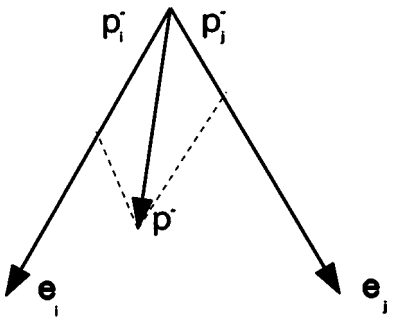

FIG. 2. Geometry of finite-range collisions.

The new state is then selected through transition probabilities. As a consequence of the small change of momentum (as compared to the CA momentum p) per time step, among the moving states only states i and j are actually attainable, so that we need to specify three probabilities only, P_o (transition to rest state) and P_i, P_j (transition to moving states i and j, respectively).

With the above procedure the momentum equation cannot be satisfied if p' exceeds the CA momentum p. An exact treatment for this alternative is described in [9]. We have adapted the latter scheme here in a simplified form.

In our heavy ion collision illustration the CA reference momentum takes the value $p=5\times10^{-15}$ g cm s$^{-1}=3\times10^{-22}$ MeV fm^{-1}; over one time step the average relative change of momentum is $\Delta\mathbf{p}/p\approx0.2$ in the experiments.

B. Translation phase

Once all momentum states have been updated by the local and finite-range collision rules, each particle, of new momentum $\mathbf{p}''$ at time step $t+1$ [Eq. (12)], is given a displacement in accordance with the equation

$$\Delta\mathbf{r}=\frac{\mathbf{p}''}{m}\Delta\tau; \tag{13}$$

a particle in a moving state i is thereby shifted from its current position in cell $\mathbf{r}$ to the nearest neighbor cell in the direction of $\mathbf{p}''$; if it is in a rest state, then it remains in cell $\mathbf{r}$.

The computation of the CA configuration at time step $t+1$ is completed once all particle positions have been updated.

IV. THERMODYNAMIC TREATMENT

We discuss in this section the construction of the thermodynamic properties associated with the CA gas of a finite number A of particles, once the particles are in a statistically stationary state.

We view this gas as a simple one-component homogeneous thermodynamic system obeying Callen's or Tisza's axiomatics of thermodynamics [10,11]. The entropy per particle, S/A, is then expressible as a function of the internal energy per particle, E/A, and the volume per particle, v/A. Accordingly, our thermodynamic system is fully determined if we are given two equations of state, for instance, temperature and pressure, as functions of the energy and volume per particle, $T=T(E/A,v/A)=T(E,v,A)$ and $P=P(E/A,v/A)=P(E,v,A)$. These equations of state are accessible from the CA simulations. A full thermodynamic description of the CA gas in its statistically homogeneous phase is thereby directly accessible in principle.

This homogeneous state is stable provided that the entropy S is maximum, i.e., provided that

$$\left(\frac{\partial P}{\partial v}\right)_T<0 \quad \text{and bounded,} \quad c_v>0 \quad \text{and bounded,} \quad \text{etc.} \tag{14}$$

The violation of a stability condition is indicative that the system ceases to conform to our initial assumption of spatial homogeneity. The configuration then undergoes a phase transition towards an inhomogeneous state.

A. Equations of state

To construct the two required equations of state the CA dynamics of the collection of particles is solved according to the following procedure.

A fixed number A of particles and a fixed ''volume'' v (a finite area of the CA lattice) are chosen so that the overall number density $n=A/v$ is fixed as well. The system of particles is further given a fixed total energy E. Since the particle mechanics adopted is conservative, the energy remains fixed. The statistical equilibrium thereby conforms to a microcanonical equilibrium.

A ''thermodynamic run'' consists in solving the CA dynamics for given A, v, and E, over a large enough number Θ of time steps. The initial conditions are prepared as follows. (a) The particles are distributed over the available ''volume'' v, according to a selected rule of positions R_{pos}; the initial potential energy $W(0)$ can then be computed. (b) Each particle is then assigned a dynamic state (rest state 0 or moving state 1,2, . . . ,6) according to some rule of velocities R_{vel}; the initial kinetic energy $K(0)$ is thus determined as well.

Accordingly, the total energy E is known for the thermodynamic run.

Suppose that the CA dynamics reaches a state of thermal equilibrium after Θ_0 time steps. The macroscopic thermodynamic variables are then generated from the corresponding microscopic CA variables via time averaging, indicated by $\langle\ldots\rangle$, over the available statistical equilibrium range, namely, the time interval (Θ_0,Θ). Temperature is the time-averaged kinetic energy per particle,

$$T=T(E,v,A)=\frac{1}{A}\langle K\rangle. \tag{15}$$

Pressure is evaluated from the (2D) virial expression,

$$P=P(E,v,A)=P_{\mathrm{g}}+P_{\mathrm{int}} \tag{16}$$

with

$$P_{\mathrm{g}}=\frac{1}{v}\langle K\rangle=\frac{A}{v}T\geqslant0, \tag{16a}$$

$$P_{\mathrm{int}}=-\frac{1}{2v}\sum_{j=1}^{A}\left(\sum_{k>j}^{A}\langle r_{jk}F(r_{jk})\rangle\right), \quad r_{jk}=|\mathbf{r}_j-\mathbf{r}_k| \tag{16b}$$

The component P_{int} is the effect of the interactions between the particles [$F(r_{jk})$, force acting between pair (j,k) along the direction $\mathbf{r}_{jk}$, given by Eq. (2) by a forward difference; for a pair in the same cell $\langle r_{jk}F(r_{jk})\rangle$ is given by Eq. (2a)].

If the thermodynamic run is repeated for a range of A, v, and E values, a detailed thermodynamic description of the equilibrium states of our particle system becomes available through the equations of state (15) and (16).

B. Comments on the thermodynamic model—phase transitions

The typical pair-interaction potentials we have in mind are assumed to be repulsive at small enough interparticle distance r, attractive at some larger distance and zero at large enough distances [cf. Eq. (2)]. Provided that the repulsion is strong enough for $r<r_{\text{rep}}$ the virial pressure relation in form (16b) indicates in the first place that the thermodynamic stability conditions may be violated through a singularity (tendency to incompressibility). In fact, take a collection of a fixed number A of particles contained in a cylinder closed by a movable piston, and kept at a constant temperature T; as the volume v is decreased, once the density exceeds the critical number density n_{rep} at which the average distance of pairs of particles approaches the critical distance r_{rep}, the system of particles tends to become incompressible.

In the second place, suppose we generate an initial configuration of particles randomly distributed over the available volume, with a density n. Provided that the density is not too low, a significant fraction of the number of occupied cells occur in ''clusters'' of different sizes s (collections of s contiguous nonempty cells). Moreover, if the density exceeds a critical density n_{P}, then a percolation phase transition takes place in the initial distribution; namely, ''percolation clusters'' of arbitrarily large sizes are then formed (cf. [12]).

Let $T_{\text{pair}}(n)$ denote the critical temperature of pair stability, at which the average kinetic energy per pair is close to the binding energy of a pair. At low enough temperatures, $T\ll T_{\text{pair}}(n)$, a cluster is a dynamically stable physical unit; it is a physically bound structure; once formed it will continue on average to exist as a stable cluster. Alternatively, at high enough temperatures, $T\gg T_{\text{pair}}(n)$, at every time step clusters are likewise observable provided only that the density is not too low (cf. the remarks about the initial state); however, these clusters are just geometrical accidents; they are not physically bound structures; they form and dissolve again, but in such a way that at any time step a same fraction of the total number of occupied cells belongs to geometrical clusters.

Hence the behavior of the pressure can be anticipated. At high temperatures [$T\gg T_{\text{pair}}(n)$], the pressure (rate of change of momentum of the free components colliding with a unit ''surface'') is manifestly the standard kinetic gas pressure P_{g} [Eq. (16a)], the free components being the individual particles; the interaction effect P_{int} [Eq. (16b)] is negligible.

At lower temperatures and for sufficiently low densities ($n\ll n_{\text{rep}}$) the bound clusters play the parts of the free particles; since their number is smaller than the actual number of particles, we expect a decrease of the actual pressure with respect to the gas pressure.

Finally, at low temperatures, if the density is increased ($n\approx n_{\text{rep}}$), the contribution of the repulsion effect to the interaction component P_{int} becomes dominant, and the pressure P becomes large.

Whether an intermediate range materializes in an actual experiment, in which the pressure is measurably less than P_{g}, will depend on the values of the parameters of the potential.

V. ILLUSTRATION: NUCLEAR FRAGMENTATION

A. General comments

The analysis of heavy ion collisions in nuclear physics in lower energy ranges (avoiding excitation of the nucleons and creation of new particles) [13–17] has raised a number of problems, among which we mention only the following: Can the formation of clusters of nucleons following the collision process be interpreted in terms of a phase transition? Is a thermodynamic phase transition consistent with a power-law distribution of the fragments (exponent 2.2 in real laboratory experiments)?

In the theoretical treatment we should ideally follow the full dynamics of the heavy ion reaction process. We may regard the latter as a sequence of three phases: (i) the initial impact of the projectile with the target nucleus, (ii) the sharing of the impact energy among the individual nucleons in a ''compound nucleus,'' possibly followed by a statistical equilibrium state, and (iii) the eventual decay of the compound nucleus into nuclear fragments.

Currently adopted theoretical methods concentrate on step (ii) and an incipient phase (iii). Phase (ii) is assumed to be sufficiently long-lived so that an efficient energy exchange can take place among the individual particles. This step is investigated by two classes of approach.

Class (1) procedures are rooted on a first implicit assumption that the system of nucleons, occupying a given available volume, is in a statistically stationary state; this state can therefore be described by standard thermodynamic methods; the statistical mechanics of the system (microcanonical or canonical ensembles) is then simulated by Monte Carlo techniques [18–21], or, in the case of simple enough interaction schemes, by semianalytical methods (cf. [1,4–7,22]). Clusters of nucleons are then isolated by various cluster-identification algorithms (minimum spanning tree, etc) [23], and a distribution function is derived. The second implicit assumption of the method is that the observed cluster-size distribution in the stationary state is identical with the distribution of the nuclear fragments of step (iii), and hence comparable with the distribution of real experiments.

Class (2) procedures handle the dynamics of the individual nucleons on the (less stringent than class 1) implicit assumption that initially the nucleons of both colliding nuclei are randomly distributed over the given volume. The dynamics of the individual particles is then followed, for instance, in the framework of CMD [2,24]. The system is found to evolve towards a statistical equilibrium whose global properties are obtained via time averaging. The methods proceed as under (1).

Additional methods have been devised to deal with different energy ranges (cf. cascade models [25] at high energies, hydrodynamic models [26]).

Class (1) methods cannot be extended to treat steps (i) and (iii); the validity of the implicit assumptions required to treat

step (ii) alone cannot be tested within this method. On the other hand the method of class (2) currently favored in the literature, namely, CMD, could be adapted, in principle, to cover the full sequence (i), (ii), and (iii), provided only that enough computer time be invested.

The CA method of this paper supplies an alternative method of class (2) capable of handling the dynamics in a computationally efficient way.

B. Construction of the thermodynamic runs and tests

Our numerical experiments are organized as follows. In conformity with laboratory fragmentation experiments the number of particles A is set equal to 300 in the majority of our CA simulations. A few test runs were carried out with $A=600$ and 900 particles, in order to assess the influence of the particle numbers on the fluctuations of the computed thermodynamic variables.

We have explored particle number densities n in the range of 0.03 to 0.10 particle/fm^2. The range of the energies E extends from -5000 to $+2500$ MeV; it is examined with a step of 50 to 100 MeV; the thermodynamic relations, and temperature and pressure against energy are thus defined with some 100 directly computed points each. The number of timesteps $\Theta=1200$, with $\Theta_0=1000$.

In our experiments two sets of rules R_{pos}, and R_{vel} defining the construction of initial conditions are adopted. (a) R_{pos1}: random uniform spatial distribution of the particles over ''volume'' v; R_{vel1}: random uniform distribution of states (equiprobability of all states). For $A=300$, rules (a) thus lead to spatially homogeneous high energy (≈ 2500 MeV) configurations. (b) R_{pos2}: approximately circular subarea of v populated with a density $n=1$ particle/cell; R_{vel2}: 90% of the particles are in the rest state, 10% are uniformly distributed over the moving states. Rules (b) produce low energy configurations, which are macroscopically inhomogeneous (except if the subregion coincides with v).

For given parameters A, v, and hence n, an initial configuration is generated by (a) [(b)] whose energy E is computed.

A first thermodynamic run is followed over $\Theta=1200$ steps, and the temperature and pressure is obtained from averaging over the last 200 steps. The thermodynamic run thus defines one ''thermodynamic point,'' A, v, E, T, and P.

A second thermodynamic run, with corresponding ''thermodynamic point,'' A, v, $E+\Delta E$, T', and P' is then prepared adopting as initial condition the last configuration of the previous thermodynamic run in which one randomly selected moving [rest] particle is stopped [set it in motion] if the previous run corresponds to rules (a) [(b)].

This procedure is continued until the energy range of interest (-5000 to 2500 Mev) has been explored.

Then a second sequence, a third sequence, etc. of thermodynamic runs is similarly prepared, starting with different initial ''volumes,'' v', v'', ...

From the table of numerical results we can plot one thermodynamic variable x_1 against a second thermodynamic variable x_2 the remaining three variables being held constant (x_1, x_2, x_3, x_4, and $x_5=A$, v, E, T, and P)

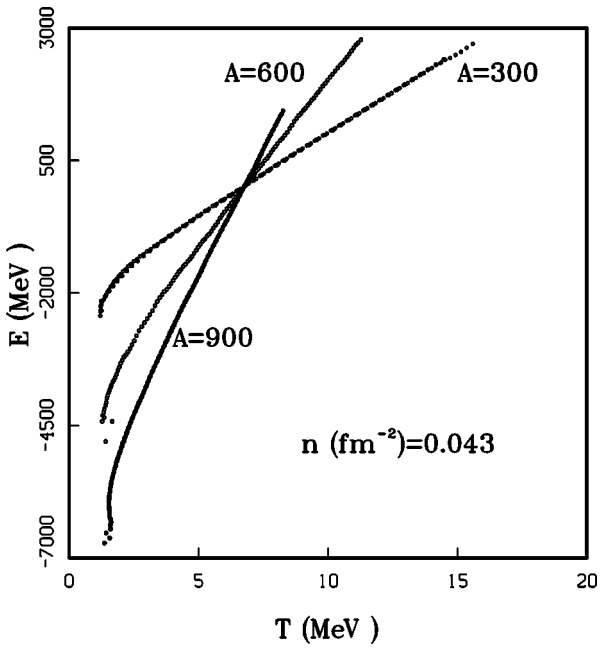

FIG. 3. Caloric curve at high enough temperatures; $n=0.043$; $A=300$, 600, and 900.

The following test calculations were performed. In a first series of auxiliary experiments at $T=5$ Mev and for $n\approx 0.05$ nucleon/fm^2, we have verified that the time averages are equivalent to phase-space averages. To this end we followed a single particle over $\Theta=2000$ time steps, and we kept track of the number of steps over which the particle was in the rest state Θ_r and in motion $\Theta_m=\Theta-\Theta_r$, respectively. Alternatively, we counted the total number of particles at rest and in motion, A_r and A_m, respectively, in a relaxed state at time step 2000. Under conditions of ergodicity, we should observe the equality $\Theta_r/\Theta\equiv A_r/A$. Our experiments indicate that we do satisfy the equality within a relative error of the order of 7–8%, consistent with the theoretically expected finite number fluctuations (of order $1/\sqrt{A}\approx 6\%$).

In the second place, at the average density of the investigated range, $n\approx 0.05$ nucleon/fm^2, we have verified in greater detail that the ideal gas law holds for $T>5$ MeV. Figure 3 displays the E-T behavior for $A=300$, 600, and 900 particles. In the range of positive internal energies, the energy shows an asymptotically linear dependence on temperature, which can be represented in the form

$$E=AT-E_o(A); \tag{17}$$

the shift of the origin $E_o(A)$ is an interaction contribution. The slopes obtained from a least squares fit are 298, 648, and 974, respectively (ideal gas values: 300 ± 17, 600 ± 24, and 900 ± 30). Over the range of validity of the linear approximation [Eq. (17)] the experimental points show virtually no fluctuations. In contrast, at lower temperatures (range 1.4–2 MeV), we observe large fluctuations. The potential contribution is found to be approximately proportional to the number of particles, $E_o(A)=7.2A$ MeV. In the third place, we have also examined the P-T relation at the density, $n\approx 0.05$ nucleon/fm^2, which should be independent of A in the ideal gas range. The numerical results indicate that within

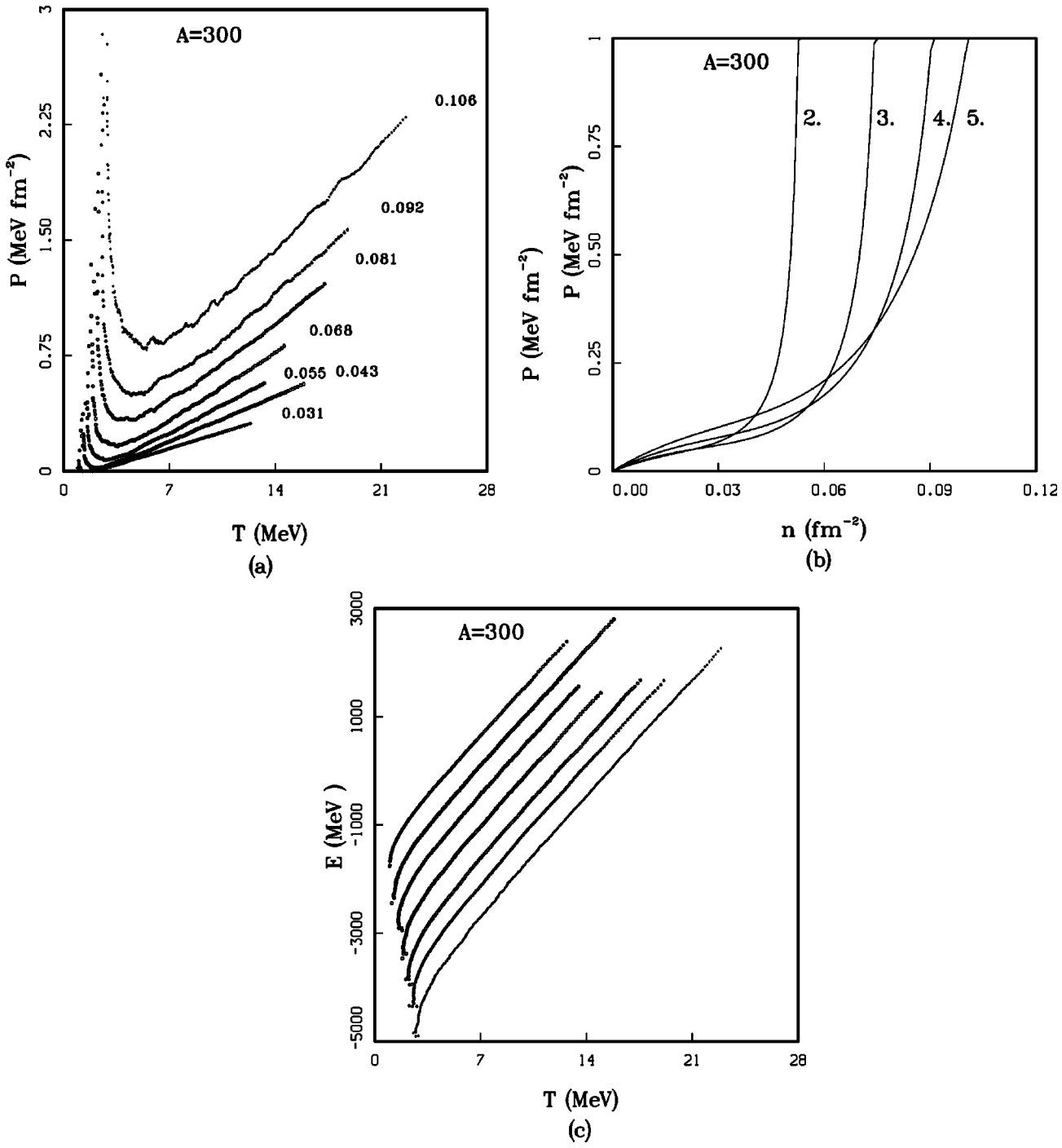

FIG. 4. $A=300$: (a) P-T relation at 7 densities $0.03 \leqslant n \leqslant 0.10$ nucleon/fm^2 (all points experimental), (b) P-n relation at four temperatures (interpolation), and (c) E-T relation at seven densities.

the statistical fluctuations the three curves superpose and appear to be practically independent of the number of particles A over the full range. As anticipated in our general discussion, the P-T relation does exhibit a vertical asymptote at a critical temperature T_{pair}; at high temperatures it follows an ideal gas law behavior; in the intermediate range, we do not observe a decrease in pressure with respect to the ideal gas law (cf. our general discussion); the interaction energy we are working with seemingly does not exhibit this behavior.

C. Thermodynamic results

The survey of the explored energy and density range is summarized in Figs. 4. All results of this section refer to $A=300$ particles.

Figure 4(a) shows the equation of state $P=P(T,n)$ in a pressure-temperature diagram, at seven densities, $n=0.031$ (bottom curve), 0.043, 0.055, 0.068, 0.081, 0.092, and 0.106 (top curve) particles/fm^2 (300 particles distributed over 2704, 1996, 1521, 1225, 1024, 900, and 784 cells, respec-

tively). All individual points of this diagram are actual computed points; no interpolations or smoothings have been applied at this stage.

Each curve has a hyperbolic shape with one asymptote coinciding with the ideal gas contribution [Eq. (16a)], the other corresponding to a constant temperature. Analytically we can interpolate this behavior by an equation of the following form:

$$P(T,n)=nT+P_o(n)+\frac{P_1(n)}{\frac{T}{T_{\text{pair}}(n)}-1}; \tag{18}$$

the functions $P_o(n)$, $P_1(n)$, and $T_{\text{pair}}(n)$ are represented as lowest-order polynomials:

$$P_o(n)=\sum_{k=1}^{4} P_{ok}n^k, \quad P_1(n)=P_{11}n, \quad T_{\text{pair}}(n)=T_1 n, \tag{18a}$$

with the coefficients taking the values

$$P_{o1}=-1.37, \quad P_{o2}=-40.2, \quad P_{o3}=388,$$

$$P_{o4}=2306, \quad P_{11}=1.51, \quad T_1=33.$$

In representation (18) the first and second contributions of the right-hand side are the counterparts of the contributions to the internal energy in the high-temperature regime [Eq. (17)]; the third contribution describes the low-temperature asymptotics.

With the help of interpolation formula (18) we replot the equation of state as a pressure-density curve, even though the numerically explored density range, 0.03 to 0.1 nucleon/fm^2, was sparsely sampled by our actual thermodynamic runs. The results are shown in Figs. 4(b) (temperatures: 2, 3, 4, and 5 MeV). As transpires from the analytic representation, at any temperature T we have a corresponding critical density, $n_{\text{pair}}(T)=0.03T$ [Eq. (18)], at which the nuclear matter becomes incompressible (diverging pressure).

Figures 4(c) show the caloric curve, energy E against T, for the seven densities (lowest density: top curve; highest density: bottom curve); all points of this curve are again computed points. We can interpolate these curves by an analytic expression,

$$E(T,n)=AT+E_o(n)+\frac{E_1(n)}{\frac{T}{T_{\text{pair}}(n)}-1}, \tag{19}$$

with

$$E_j(n)=E_{jo}+E_{j1}n, \quad j=0,1$$

$$E_{oo}=-195, \quad E_{o1}=-4.4\times 10^4, \tag{19a}$$

$$E_{1o}=-17.7, \quad E_{11}=-325;$$

$T_{\text{pair}}(n)$ being defined in Eq. (18a).

Equations (18) and (19) exhibit a singularity in the behavior of the pressure and the energy, at the critical temperature $T=T_{\text{pair}}(n)$. The latter roughly corresponds to an average kinetic energy per particle close to (but slightly lower than) the binding energy of a particle in a stable pair Sec. (IV B).

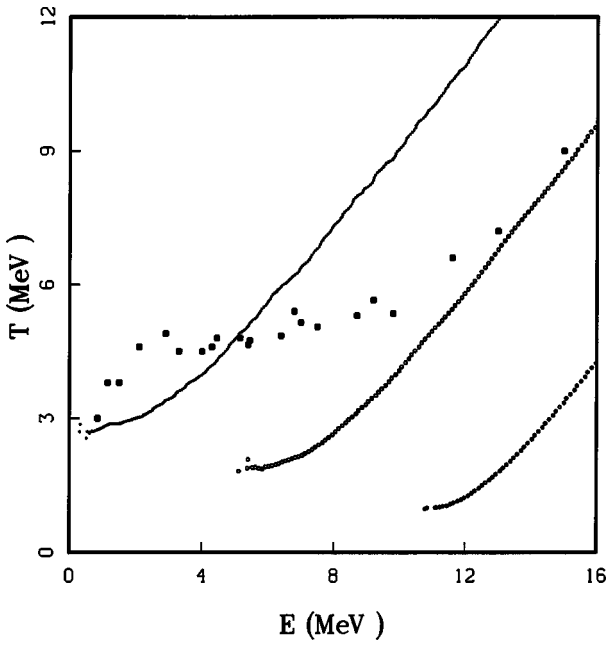

FIG. 5. Theoretical caloric curve (2D) E-T at $n=0.03$, 0.06, and 0.10 (E, rescaled, in MeV/nucleon and n in fm^{-2}) compared with laboratory experiments (3D) [27].

Although our numerical experiments are two-dimensional, and hence, the results are not directly comparable with real laboratory experiments, we wish to point out that a plateau in the T-E curve has been reported in the collisions of gold-gold and oxygen-silver ions [27], in a temperature range 4–6 Mev. In our numerical experiments the T-E curve likewise exhibits a plateau [the asymptote in E-T relation (19)]; the relevant temperature is $T_{\text{pair}}(n)\approx 3$ Mev [Eq. (18a)] for the higher densities we have considered. Figure 5 shows the superposition of the experimental points with our theoretical caloric curve at $n=0.03$, 0.06, and 0.1 particle/fm^2. Our theoretical result is thus not only qualitatively consistent with this experimental result, but even quantitatively the theoretical and experimental orders of magnitude of the critical temperature range are compatible. It should be kept in mind, however, that an experimental determination of a nuclear temperature remains a controversial operation.

D. Formation of clusters

Figures 6 supply plots of the microscopic distribution of the particles over the available CA ''volume'' v at different densities and energies (or temperatures).

(i) At the lowest density level investigated, $n\approx 0.03$ particle/fm^2, and (ii) at a high enough temperature ($T>1$ Mev) or energy ($E>0$), all particles remain free. The medium is seen to be uniformly populated at any time step ($>\Theta_0$). Snapshots taken at random time steps may exhibit a few filamentary clusters of small size ($s\leqslant 5$), but these structures dissolve at the following time step. The configuration is thus virtually an ideal gas. (b) As the temperature and energy are lowered we finally observe stable, relatively small sized energetically bound aggregates ($s\approx 30$ at $E\approx -700$ MeV).

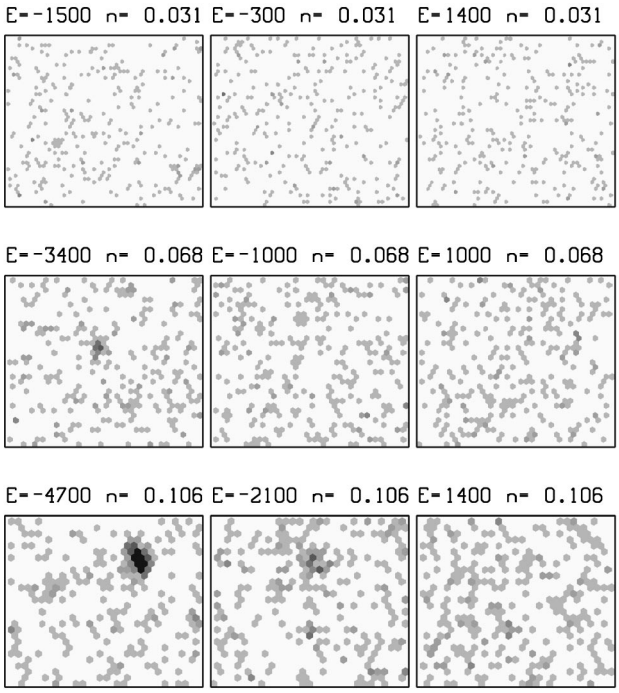

FIG. 6. $A=300$: Microscopic distribution of nucleons over the CA cells at different densities and energies; condensation aggregates observed at high densities and low energies.

The majority of the particles remain free, even at energies <-1000 Mev. The proper investigation of the thermal equilibrium is time consuming at these low densities, since collisions are too rare.

(ii) At intermediate densities, $n\approx 0.05$ particle/fm^2, we notice again that (a) at high energies and temperatures $E\approx 1300$ and $T\approx 9$ MeV, most particles remain free, although we observe now longer filaments ($s\approx 10$); statistically the medium remains homogeneous. (b) As the energy and temperature are lowered, several large bound aggregates develop, which may contain over 30 particles (at $E=-2000$ Mev); typically, as the energy is further decreased, we observe a single large aggregate that finally tends to dominate. At this stage the macroscopic translation symmetry may appear as broken; in the limited context of our experiments, the medium appears as inhomogeneous. However, in the strict thermodynamic context, that corresponds to the limits $A\to\infty$, $v\to\infty$, with $n=A/v$ remaining finite, this is not the case; in this infinite nuclear medium homogeneity is preserved on a small scale (even though this scale is now larger than the original scale of homogeneity). (iii) At the highest densities investigated, $n\approx 0.1$ nucleon/fm^2, we observe (a) already large aggregates ($s\approx 30$) at high energies ($E=1500$ MeV), which remain uniformly distributed over the lattice of cells and which are surrounded by clusters of smaller sizes. These clusters do not appear to be energetically bound. Pictures of the microscopic configuration at successive steps in time show that they dissolve and that new clusters form. In fact, the ideal gas properties continue to be obeyed in spite of the apparent statistical equilibrium between cluster formation and dissolution. (b) At low energies and temperatures a single dominating energetically stable aggregate is observed (with $s>100$ at $E=-5000$ MeV). The latter is surrounded by stable clusters of all sizes. In terms of nuclear physics, we now observe a thermodynamically stable distribution of nuclear fragments of all sizes up to a maximum size.

The visualization of the spatial distribution of the particles within the accessible ''volume'' v (Fig. 6) confirms that our *N*-body system of nucleons exhibits *two phases*, as anticipated in our comments Sec. (IV B) on general grounds. At low densities and high enough temperatures the system behaves essentially like a perfect gas whose particles are the individual nucleons. At high densities and low enough temperatures we observe a gas whose particles are aggregates or clusters of nucleons. Accordingly, at fixed temperature T (in an appropriate range), if we let the density increase from a low enough to a high enough value, we expect to encounter a critical density $n_P(T)$ at which a phase transition from a gas phase to an aggregation phase takes place. In fact, percolation and aggregation-type phase transitions are well known to occur at well-defined critical densities. Alternatively, then, at fixed density n, if the temperature drops from a high enough to a low enough value, this transition occurs at a critical temperature $T_P(n)$; for dimensional reasons this critical value is of the order of the binding temperature of a particle in a pair [but slightly higher than the critical temperature $T_{\rm pair}(n)$ entering Eqs. (18) and (19)].

Close to the critical temperature $T_{\rm pair}(n)$ [Eqs. (18) and (19)] thermalization is very slow, so that the numerical results may not be fully reliable; therefore, we have not investigated the thermodynamics in the temperature range $T<T_{\rm pair}(n)$ [or the density range $n>n_{\rm pair}(T)$]. Intuitively it seems likely that the latter range corresponds to a condensed phase in which all clusters have merged into a single supercluster.

The aggregation-type phase transition itself occurs at a higher temperature (or lower density). The existence of the latter is expected to manifest itself in the occurrence of a cluster distribution in the form of a power law.

E. The distribution of the fragments

Figures 7 show the cluster distributions at $n=0.1$ particle/fm^2, namely $N(s)$, the number of clusters against s, the cluster size, in a log-log plot [energies -4400 MeV (a), -3600 MeV (b), and 2500 MeV (c)]. In Figs. 7(a) and 7(b) the representative points are seen to follow a straight line. Hence the distribution obeys a power law,

$$N(s)\propto s^{-\tau} \tag{20}$$

with $\tau\approx 1.35$. This distribution compares favorably with the 2D results of discs obtained by Strachan and Dorso, who find $\tau=1.4$ [23].

At the higher energies (2500 Mev) a curvature becomes noticeable in these plots. Likewise, if we consider lower densities, a curvature essentially survives at all energies investigated.

A fragment distribution conforming to Eq. (20) describing the occurrence of aggregates of all sizes is the fingerprint of a percolation phase transition [12] or an aggregation-type phase transition. The numerical results of Fig. 7 are indicative that the power-law behavior is exactly obeyed at some energy intermediate between alternatives Fig. 7(a) and 7(b), i.e., close to the energy at which the caloric curve shows a

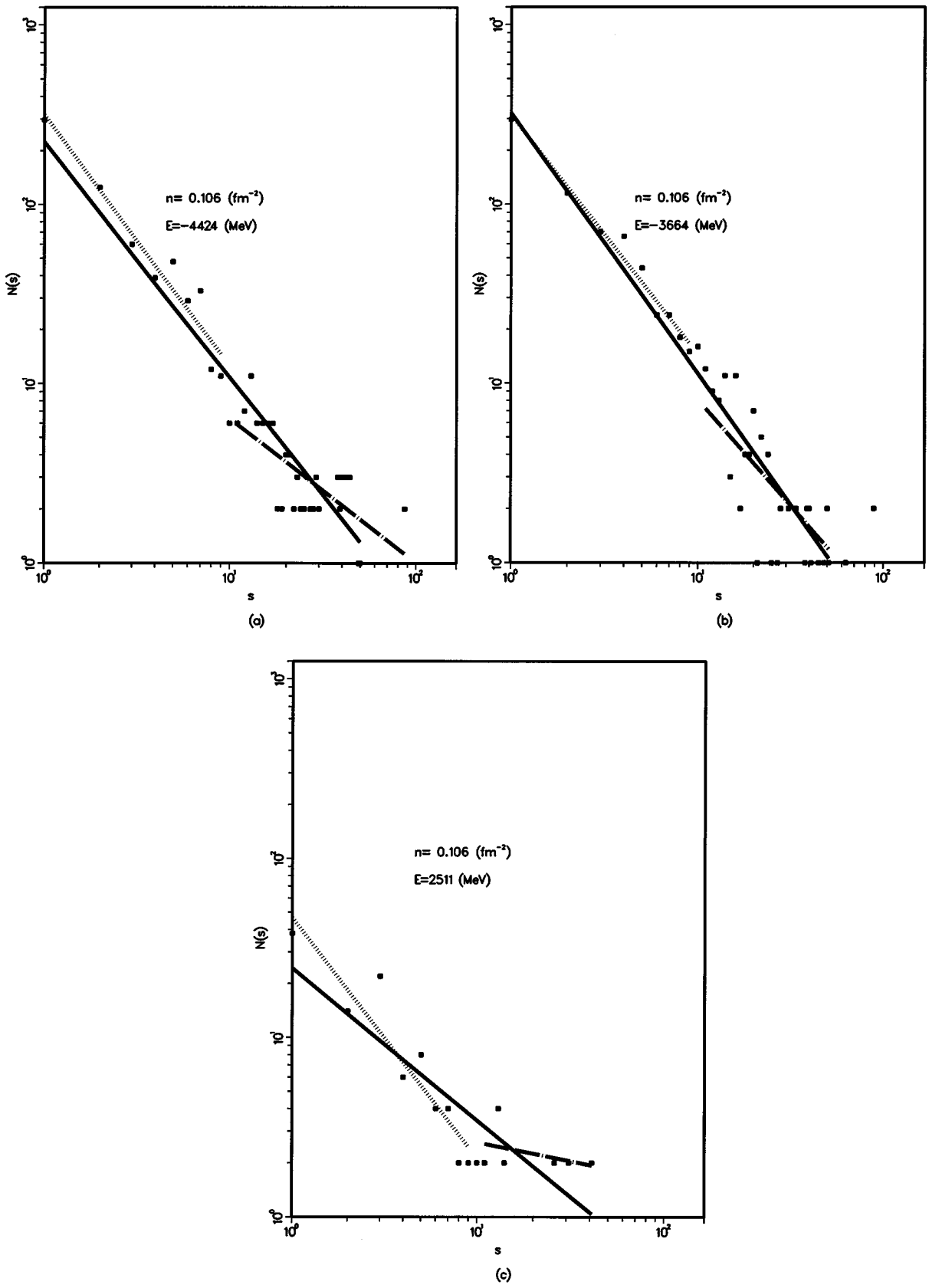

FIG. 7. Cluster distribution at $n=0.1$; $E=-4400$ (a), -3600 (b), and $+2500$ MeV (c) (14 runs). Least-squares estimates of τ (a) full s range (continuous line), 1.32; $s<10$ (dotted), 1.40; $s>10$ (dashed): 0.80; (b) 1.45, 1.34, and 1.18 and (c) 0.85, 1.34, and 0.21, respectively.

bent [Fig. 4(c)]. On the other hand, under alternative Fig. 7(c) we notice that there are no large aggregates; the clusters are not physically bound; they dissolve and new clusters form again.

Our numerical investigation thus supports the idea of an aggregation-type phase transition which is responsible for the nuclear fragment distribution in real (3D) laboratory experiments. The fragments of heavy ion collisions are indeed found to obey a power law of exponent $\tau = 2.2$. The difference between the laboratory value and the value derived from our 2D numerical experiments is an effect of the dimensionality.

VI. CONCLUSION

In this paper we have developed a simple 2D cellular automaton describing *N*-body systems. From the direct dynamical results global statistical properties can be introduced. In particular thermodynamic properties are easily derived [Eqs. (16)].

As an illustration the model has been applied to the problem of heavy ion collisions in nuclear physics, with the resulting fragmentation of the nuclear matter. The model results, which are two-dimensional, are in qualitative agreement with the real experiments (three-dimensional). They suggest an aggregation-type phase transition that determines the distribution of nuclear fragments, occurring at a low temperature. Since the direct purpose of this paper is to demonstrate the application of CA approaches to *N*-body dynamics rather than to phase transitions, we have not concentrated here on a precise analysis of the aggregation phenomenon. We plan to come back to this problem. For the purposes of comparison of the CA approach with laboratory experiments we are currently carrying out a three-dimensional extension of the method. We further plan to deal with the full collision process of the two ions, an approach that should allow us to dispense with the thermodynamic assumptions implicit in the current treatment. In the latter approach the distribution of the fragments can be read off directly from the numerical results without resorting to sophisticated cluster identification methods. A major aim of the extension will consist in a comparison of the dynamical results with the results obtained by Monte Carlo simulations.

ACKNOWLEDGMENTS

A.L. would like to thank the SPM Department of the CNRS (Paris) for financial support of a stay at LPT in Strasbourg during which this work was initiated. He thanks the members of LPT for the hospitality extended to him, as well as the members of the Supercomputing Center CINECA in Bologna where part of the numerical work was done. J.P. gratefully acknowledges financial support from the Royal Society-FNRS European Exchange program (1997, 1998).

[1] X. Campi and H. Krivine, Nucl. Phys. A **620**, 46 (1997).
[2] P. Finocchiaro, M. Belkacem, J. Kubo, V. Latora, and A. Bonasera, Nucl. Phys. A **600**, 236 (1996).
[3] J. Hardy, O. de Pazzis, and Y. Pomeau, Phys. Rev. A **13**, 1949 (1976).
[4] T. S. Biro, J. Knoll, and J. Richert, Nucl. Phys. A **459**, 692 (1986).
[5] S. K. Samaddar and J. Richert, Z. Phys. A **332**, 443 (1989); Phys. Lett. B **218**, 381 (1989).
[6] J. Pan and S. Das Gupta, Phys. Lett. B **344**, 29 (1995).
[7] S. Das Gupta and J. Pan, Phys. Rev. C **53**, 1319 (1996).
[8] C. J. Joachain, *Quantum Collision Theory* (North-Holland, Amsterdam, 1983).
[9] J. Perdang in *Cellular Automata: Prospects in Astrophysical Applications*, edited by J. M. Perdang and A. Lejeune (World Scientific, Singapore, 1993), p. 342.
[10] H. B. Callen, *Thermodynamics* (Wiley, New York, 1960).
[11] L. Tisza, *Generalized Thermodynamics* (MIT Press, Cambridge, MA, 1966).
[12] D. Stauffer, *Introduction to Percolation Theory* (Taylor & Francis, London 1985).
[13] See Refs. [1] in Ref. [2].
[14] J. Pochodzalla *et al.*, Phys. Rev. Lett. **75**, 1040 (1995).
[15] J. A. Hauger *et al.*, Phys. Rev. Lett. **77**, 235 (1996).
[16] H. F. Xi *et al.*, Phys. Rev. C **58**, R2636 (1998).
[17] M. B. Tsang *et al.*, Phys. Rev. C **55**, R557 (1997).
[18] W. Janke and S. Kappler, Phys. Rev. Lett. **74**, 212 (1995).
[19] P. Labastie and R. L. Whetten, Phys. Rev. Lett. **65**, 1567 (1990).
[20] A. Hüller, Z. Phys. B **93**, 401 (1994).
[21] D. H. E. Gross, Phys. Rep. **279**, 119 (1997).
[22] W. Bauer, D. R. Dean, U. Mosel, and U. Post, Phys. Lett. B **150**, 53 (1985).
[23] A. Strachan and C. O. Dorso, Phys. Rev. C **56**, 995 (1997).
[24] J. Aichelin, G. Peilert, A. Bohnet, A. Rosenhauser, H. Stöcker, and W. Greiner, Phys. Rev. C **37**, 2451 (1988).
[25] D. l'Hôte and J. Cugnon, Review of Nucl. Phys. **5**, 37 (1991).
[26] H. Stöcker, W. Greiner, Phys. Rep. **137**, 277 (1986); R. B. Clare and D. Strottmann, *ibid.* **141**, 177 (1986).
[27] NUPECC Report: Nuclear Physics in Europe, edited by J. Vervier *et al.*, 1997 (unpublished).